The crystal ball, the spider and other stories: a journey around the test tower of the M4 adaptive mirror

Briguglio, Runa, Pariani, Giorgio, Xompero, Marco, Tofani, Beatrice, Rossetti, Marco, et al.

Runa Briguglio, Giorgio Pariani, Marco Xompero, Beatrice Tofani, Marco Rossetti, Paolo Calabretto, Armando Riccardi, "The crystal ball, the spider and other stories: a journey around the test tower of the M4 adaptive mirror," Proc. SPIE 10703, Adaptive Optics Systems VI, 1070373 (11 July 2018); doi: 10.1117/12.2311334

SPIE.

Event: SPIE Astronomical Telescopes + Instrumentation, 2018, Austin, Texas, United States

The crystal ball, the spider and other stories: a journey around the test tower of the M4 adaptive mirror.

Runa Briguglio[a], Giorgio Pariani[b], Marco Xompero[a], Beatrice Tofani[a], Marco Rossetti[c], Paolo Calabretto[c], and Armando Riccardi[a]

[a]INAF Osservatorio Astrofisico Arcetri L. E. Fermi 5, 50125 Firenze Italy
[b]INAF Osservatorio Astronomico Brera, via E. Bianchi 46, 23807 Merate (LC) Italy
[c]Dipartimento di Fisica e Astronomia, Universit degli Studi di Firenze

ABSTRACT

M4 is the adaptive mirror of ELT, currently at its FDR. It is composed by 6 thin shell mirror segments, controlled by 5136 voice coil actuators. Before its installation at the telescope, it will be optically calibrated on a test facility (OTT) in Italy. The calibration includes the computation of the flattening command and the segments co-phasing, i.e. the correction of the differential piston amongst them. Given the large complexity of the deformable mirror and the very tight requests on the measurement accuracy, we set-up a risk-mitigation activity based on the laboratory demonstration of some key elements within the test tower. In this paper we present the results of the experimentation. We measured at nanometer level the interferometric cavity; we investigated how the interferometer reacts in presence of spider arms dividing the test mirror into separated islands; we integrated and tested a multi wavelength sensor to measure the inter-segment absolute differential piston; we aligned and tested for stability the pupil relaying optical system to be installed on the OTT. Such activity is performed in the AO laboratory at INAF-Arcetri in Italy, in preparation of the M4 optical calibration on the OTT, scheduled to start in 2020. The M4 project is led by the italian consortium AdOptica under an ESO contract.

Keywords: Adaptive Optics, Wavefront correctors, Deformable mirrors, Optical calibration, Laser Interferometry

1. INTRODUCTION: OPTICAL TEST OF M4, THE E-ELT DEFORMABLE MIRROR

The M4 will be the most complex, large format deformable mirror, composed by 6 petal-shaped segments, each controlled by 892 voice-coil actuators. The internal metrology device is based on capacitive sensors co-located with the actuators so that they are controlled at high frequency in a position close loop. The M4 unit is developed by the consortium AdOptica under an ESO contract.

Before its final installation on the E-ELT at Cerro Armazones, the adaptive M4 mirror will undergo a 2 years optical calibration and verification campaign. The main expected outcomes of such activity are the tuning of the internal metrology to deliver the actuator flattening command and the verification of the system performances versus the top-level requirements. INAF is involved in the project for the definition, design and performing of the optical test. Within this frame, we prepared the optical design of the test tower (OTT, extensively described in[1]), the calibration protocol[2] and the measurement error budget;[3] the test procedure has been simulated with a numerical code[4] to identify the key algorithms to manage the measurements of the segmented deformable mirror. In the last years, the techniques and procedures for the optical calibration of large format adaptive mirrors have been refined and applied on larger and/or more complex systems, such as the LBT and VLT DM. The case of the M4U presents some relevant differences with respect to the others: for instance, it is a segmented mirror, with a very large number of actuators; the test bench is composed by large optics with many degrees of freedom; at last, the flattening and phasing requirements for the measurement accuracy are very demanding. During the optical verification of the DP, the demonstration prototype of the M4U, we investigated[5] many aspects related to the

Further author information:
Runa Briguglio: E-mail: runa@arcetri.astro.it, Telephone: +39 055 2752200

Adaptive Optics Systems VI, edited by Laird M. Close, Laura Schreiber, Dirk Schmidt, Proc. of SPIE Vol. 10703, 1070373 · © 2018 SPIE
CCC code: 0277-786X/18/$18 · doi: 10.1117/12.2311334

calibration procedure, especially applied to the case of a segmented system. During the final design phase of the OTT we identified some open points that could be a potential risk for the optical measurements: for instance, how to achieve a nanometer level accuracy and how to cope with the spider arms shadow. We then defined a risk-mitigation strategy based on the laboratory verification of these issues. In the following we give an account of the laboratory activity performed in preparation of the optical tests of the M4U.

2. THE SPIDER-ARMS TEST

2.1 Spider arms shadow, islands and differential piston error

Interferometers are not sensitive to the absolute piston of the test optics, this feature being also known as *phase ambiguity*. Apart from the obvious case of a segmented optics, the test cavity may be divided into separated areas (or *islands*), for instance in presence of large spider arms. If the interferometer signal cannot be retrieved under the spider shadow, the phase reconstruction process fails in connecting the islands. In this condition, an arbitrary $n\lambda$ piston value is assigned independently to each island because of the phase ambiguity. This behaviour is a concerning issue when the islands are produced over the continuous (connected) surface of a deformable optics. In facts, the added arbitrary piston value is measured as a discontinuity on the optical surface, which is indeed continuous. This spurious signal would be then corrected with the actuators to restore the optical flatness.
If the size of the shadow is small compared to the interferometer resolution element, then the light gathered on the pixel may be enough to produce a sufficient modulation level amongst the frames needed to reconstruct the phase. In this case the shadowing will not separate the aperture into islands, although the WF will be distorted on those pixel immediately below the spider. For the case of the OTT interferometer (a 4D Technology, dynamic Twyman-Green) the resolution elements is a 2x2 *super-pixel* and the modulation signal is computed over these 4 adjacent pixels. The modulation threshold is a user-defined processing parameter, so it follows that when the shadowing is thin, lowering the modulation threshold could help in avoiding the islands effect.
The OTT has its fold mirror and diverger suspended within the beam by a spider arms system. We optimized the spider rods with a goal thickness of 2 mm. However, considering the extremely large number of frames that shall be collected during the optical calibration of the M4 unit, we need to assess the impact of the spider arm thickness, at least statistically. To this purpose we set up a laboratory test to evaluate the rate of islands errors over a continuous surface with spider arms. In order to be representative, the test shall match the final measuring conditions as in the OTT. The test was run on an optical bench suspended on dampers to reject vibration; the test cavity was as much as possible insulated from air convection, although this was not sufficiently achieved during the last run (as it will be discussed in the following).

2.2 Laboratory setup

We prepared a laboratory testbed to simulate the optical configuration of the OTT. We mounted a F/2 converging lens on the exit flange of a 4D-Technology Twyman-Green interferometer. The test beam illuminates a 50 cm diameter, F/5 spherical mirror with its center placed at the lens focus. The surface of the sphere is focused on the interferometer CCD. Thanks to the very large input beam, the final pixel scale matches the OTT one, although the return optics is much smaller that the OTT collimator.
We mounted a frame in front of the spherical mirror and prepared a set of metal rods as spider arms simulator, with thicknesses ranging from 2.2 mm to 5 mm. Given a pixel scale of 1.3mm/pix, the rods are smaller, equal or larger than the interferometer meta-pixel. A meta-pixel is a 2x2 pixel matrix of the CCD; in our pixelated mask interferometer, the meta-pixel is the resolution element where the phase signal is measured.

2.3 Data sampling and analysis

We run a set of measurements, as follows: two rods are mounted in front of the sphere, one horizontally and one at 30° from the other; the cavity is aligned to obtain $\sim$ 15 um PtV horizontal, vertical or diagonal orientation tilt, to simulate a worst vibration case (and to excite the interferometer with a high frequency signal over the pixels); a sequence of 1000 frames is captured at the interferometer frame rate.
The 4D Technology interferometer allows the collection of raw frames and the post-processing into phase-maps at a later time. We then post-processed the same raw dataset with different modulation threshold (by changing the value in the system parameters). In this way we investigate the effect of this threshold on the pixels below

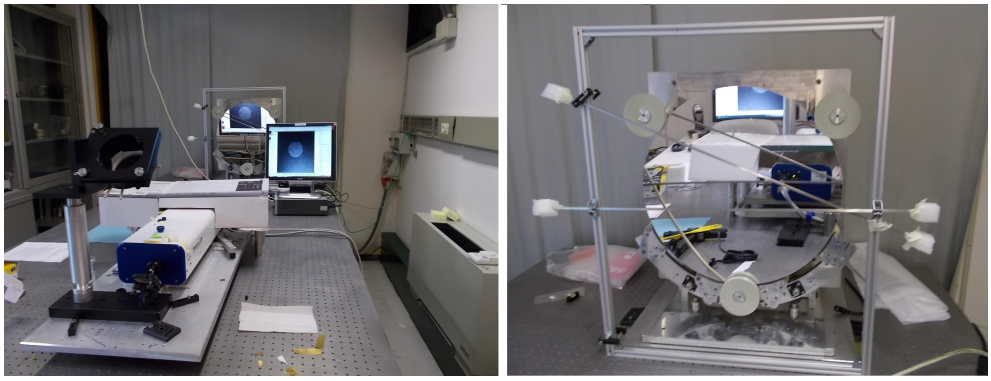

Figure 1. Laboratory setup for the spider test. On the left: the 4D interferometer with the folding mirrors to steer the beam toward the spherical mirror. On the right: the 50 cm sphere with the test rods installed.

Item	Description	Value
a	Area of the test region	20x20 pix
t_r	Reconstruction error threshold	20 nm
t_p	Piston error threshold	100 nm
λ	He-Ne laser wavelength	632 nm

Table 1. Summary of the processing parameters.

the spider. As a reference, we show a map of the typical modulation values in Fig.2, where it is clearly visible that the value below the spider is close to 0. The datasets have been processed to identify island errors and reconstruction errors in general. In particular we counted the error events for both cases, according to the following procedure:

1. for each couple of frames w_i and w_{i+1} we computed the difference $dw = w_i - w_{i+1}$.
2. we computed the RMS(dw) and compared it with an arbitrary threshold t_r: if $RMS(dw) \geq t_r$ we set $c_r = c_r + 1$, being the counter of the *reconstruction error* events;
3. we measured the mean values of $< dw_{r_j} >$ in the three measurement regions r_j as in Fig.3.
4. we computed the differences $dp0 =< dw_{r_1} > - < dw_{r_0} >$ and $dp1 =< dw_{r_2} > - < dw_{r_1} >$;
5. we then compared such differences with another arbitrary threshold t_p. If $dp0 \geq t_p$ we set $c_{p_0} = c_{p_0} + 1$ and the same for $dp1$ and c_{p_1}, being the counters of the island errors, for the two spiders respectively.

2.4 Result and discussion

In Fig. 4 we present the number of errors detected by the processing algorithm in the various cases addressed. The main result, in the perspective of the OTT activities, is that the number of island errors with a 3 mm spider (larger than the OTT one) is negligible. We may assume that with the final OTT spider (2 mm) we will not need to face with the island issue. The non-zero reconstruction errors with the 2 mm spider is due mostly to an increased convection level during the sampling (as measured off-line with a dedicated investigation) so that we conclude that the 19 occurrences are due to not-nominal measurement conditions.

3. INTEGRATION AND VERIFICATION OF THE PISTON SENSING UNIT

The six mirror segments will be co-phased in close loop with the interferometer. To overcome its intrinsic phase ambiguity, we need an external piston sensing unit, even with a relatively low precision, to bring the initial difference piston within 1 λ. Such device is the SPL, or sensor of phase lag and is composed by an illumination system (one per neighbouring shell couple) and a camera viewing at the gap between two adjacent shells. The

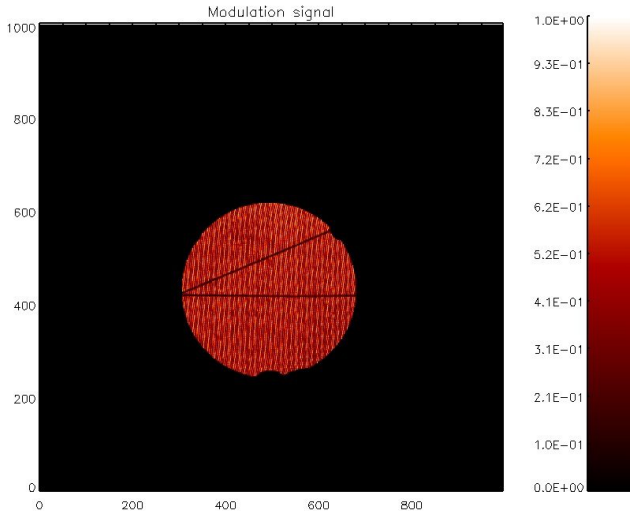

Figure 2. Map of the modulation values as read from the interferometer software. Values are zero (or close to) below the spiders.

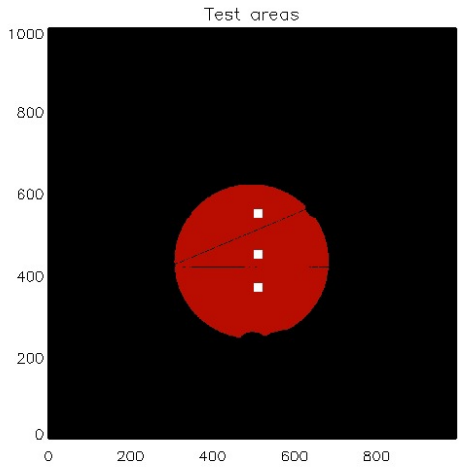

Figure 3. Location of the test areas to run the processing algorithm.

Spider Thickness	4.2 mm								
Fringes Pattern	Recons. Errors				Island Errors				
Diag.	480	411	373	500	231	219	197	191	← Rod 1
					112	91	18	4	← Rod 0
Horiz.	466	426	297	324	252	229	223	200	
					42	20	2	0	
Vert.	10	2	0	0	0	0	0	0	
					0	0	0	0	
Mod. Thresh.	5	10	15	20	5	10	15	20	

Spider Thickness	3 mm								
Fringes Pattern	Recons. Errors				Island Errors				
Diag.	32	1	1	148	0	0	0	0	← Rod 1
					1	0	0	0	← Rod 0
Horiz.	2	0	0	0	0	0	0	0	
					0	0	0	0	
Vert.	0	0	0	0	0	0	0	0	
					0	0	0	0	
Mod. Thresh.	5	10	15	20	5	10	15	20	

Spider Thickness	2 mm								
Fringes Pattern	Recons. Errors				Island Errors				
Diag.	0	0	2	19	0	0	0	0	← Rod 1
					0	0	0	0	← Rod 0
Horiz.	0	0	0	0	0	0	0	0	
					0	0	0	0	
Vert.	0	0	0	0	0	0	0	0	
					0	0	0	0	
Mod. Thresh.	5	10	15	20	5	10	15	20	

Figure 4. Table of the reconstruction and island errors as detected by the processing algorithm, arranged by fringes orientation, modulation threshold, spider thickness.

illumination system is fed by a broadband lamp coupled with a very narrow-band filter, actually a liquid crystal, tunable filter (LCTF). A camera images the PSF produced by the two shell patches illuminated; several PSFs are compared as long as the LCTF sweeps the wavelengths and the differential piston is found by fitting the PSF profile.

We arranged in the laboratory two different setups. The first is a prototype of the SPL, the second is a device to test it.

Figure 5. Design of the SPL unit.

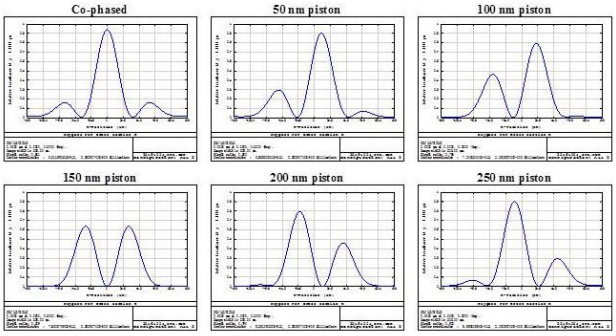

Figure 6. Overview of the expected PSF as measured by the SPL camera corresponding to various differential piston between the shells.

3.1 The SPL

The SPL concept is based on a F/70 Barlow design to measure two semi-circular patches of 12 mm diameter, across two neighbouring shells. Such optical scheme has been selected to allow the best possible sampling of the resulting PSF created by the segmented aperture. The illumination system is composed by a broadband lamp and the LCTF: we selected the band range 420 nm to 730 nm with a bandwidth (for each selected wavelength) as narrow as 3 nm. Thanks to such specification, the SPL capture range is 20 μm and its accuracy is 60 nm. Such accuracy is enough to detect initial differential piston errors larger than the interferometer λ, that cannot be correctly sampled by the interferometer because of the phase ambiguity. The SPL camera is a commercial CMOS with a 3.75 μm pixel, allowing a decent sampling of the resulting PSF. In Fig. 5 we show the system design, while in Fig. 6 we show a sample of simulated PSF versus shell differential piston.

3.2 The testing unit

The test device for the SPL is composed by a pair of glass cubes, produced by cutting a single polished piece. One of the cubes is shifted with respect to the other. Such movement is a pure translation (i.e. with no rotation) thanks to the fact that both cubes share the same base surface and interface. This is of crucial importance as the device shall be able to produce a pure piston without adding a differential tilt. Given the working principle of the SPL, in facts, even a very small (a few hundreds of nanometers) differential tilt is enough to split the resulting PSF into two and prevent the measurement. The movement is performed by a precision piezo-electric screw, with a minimum step of 25 nm. The initial differential piston is not important, as long as it is within the SPL capture range (20 μm). The alignment of the two cubes has been completed in front of the interferometer. To this purpose, we inserted a beam splitter in front of the cubes. The beam splitter acts as a 45° folding mirror for the SPL setup, arranged on a side, while the cube are continuously monitored by the interferometer. In Fig. 7 we show the laboratory setup with the cubes mounted in front of the interferometer during the initial alignment.

4. INTEGRATION AND ALIGNMENT OF THE LENS SYSTEM

4.1 The Lens System

In the OTT, the test beam from the interferometer is expanded by a parabolic collimator fed by a 1 inch, f/3 diverger. Such beam expanding group requires an additional optics to properly relay the M4 image to the interferometer CCD. This task is realized with a secondary beam expander composed by two lenses whose distance from the interferometer is adjusted to focus the M4 image. We arranged in the laboratory a demonstration setup for such lens system (LS) and we tested the alignment procedure.

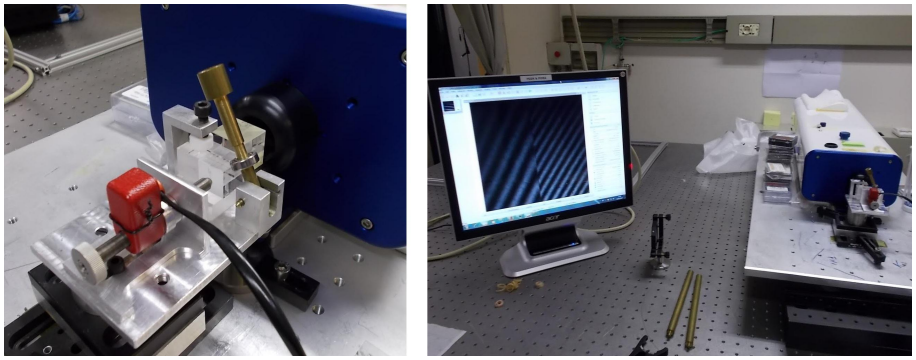

Figure 7. Left: the two cubes of the tsting unit on their mount with the beam splitter cube in front of the interferometer (the blue box). Right: the laboratory setup with the interferometer screen before the cubes fine alignment (see the differentially tilted fringes).

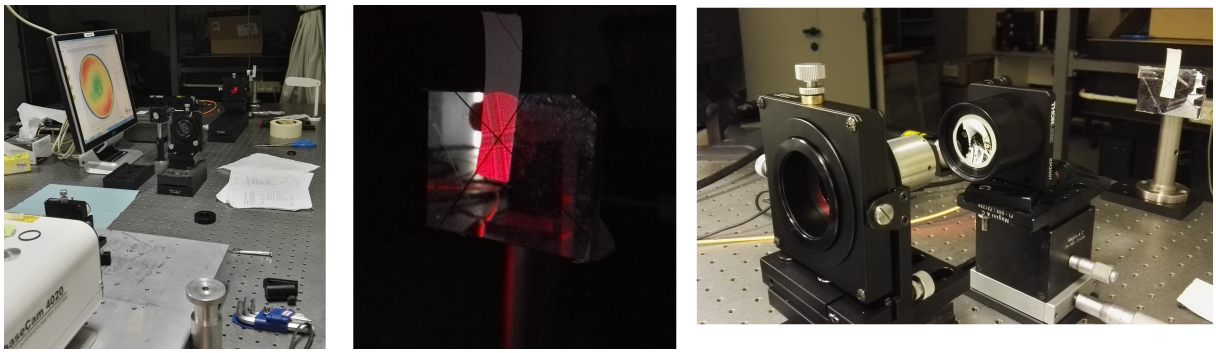

Figure 8. Test setup in the lab for the optical alignment of the LS.

4.2 Alignment procedure

The setup consists of an interferometer and three lenses which, from now on, will be called L1, L2 and L3. The alignment procedure is performed in laboratory with the elements mounted on the optical bench.Using the interferometer software, a circular mask is created and we assume that the center of this mask will mark the CCD center. An alignment tool (cross-wire) is placed on the output beam of the interferometer in order to center it with the mask previously created. A flat reference mirror M1 is placed after the nominal position of L3 and is aligned with the inteferometer: such a mirror is used to define the axis of the system. On the mirror we placed two fabric wires and adjusted them to match the CCD center, i.e. we superimpsed them to the alignment cross-wire. In order to align the mounts with the axis just created we used a pinhole placed on the translation mount of the lens L1, using the XY of the mount in order to center the lens with the center defined in the M1. The same is repeated by moving the pinhole on the mounts of the lenses L2 and L3. After the alignment of the mounts, the lens L1 is inserted. In order to center the current cross image with the center of the reference one, the L1 tip-tilt is used. The same steps are repeated after having inserted the lens L2 inside its mount. The lens L3 is mounted inside its tube, inserting a piece of paper on the mirror M1 (to visualize the cross) we adjust the L3 tip-tilt to align the 2 images of the cross. A reference sphere is mounted with its focus at the L3 focus with a kinematic mount. The sphere and the focus of L3 are moved in order to null the fringes and the defocus. The alignment is completed and the alignment tool is removed. At the end we check on the screen that the pupil is centered with respect to the mask previously defined.

5. CALIBRATION OF THE LENS SYSTEM WITH THE RANDOM BALL TEST

As mentioned above, the lens system (LS) is a converging optics composed by three lenses. It shall be accurately measured to remove its contribution from the M4 calibration. We selected the random ball test (RBT) as a suitable set-up for the measurement of the LS. After the integration and alignment of the test LS in laboratory, we arranged a RBT to practice it and to evaluate the accuracy level that can be reached.

5.1 Concept of the RBT

The RBT is a way to implement the interferometric measurement of spherical optics. A comprehensive description may be found in.[6] The core is to close the cavity with an intra-focal return sphere, which is in facts a full sphere (the Random Ball or RB). The RB shall sit on three spheres so that its center is located at the system focus. The RB may be smoothly rotated, sliding over the supporting spheres. For any movement, a different surface patch is sampled, while the optical alignment is preserved thanks to the sphere symmetry. It is then possible to sample a very large number of frames while the RB is rotated. It follows that after averaging n frames, the final measurement error may be estimated as $\sigma_{RB}/\sqrt{n}$, where σRB is the typical WFE of the RB over the patch. To ensure a robust statistics, the measurements shall be un-correlated: however, it is enough that this condition is satisfied pixel-wise, i.e. two patches shall be separated by a few pixels. RB are commercially available components, with a typical surface irregularity of the order of 50 nm RMS (on the small measurement patch). A final measurement accuray better than $\lambda/100$ may be achieved with a few hundreds frames.
The RB shall be initially aligned to close the optical cavity, so that the alignment modes (coma and power) cannot be measured.

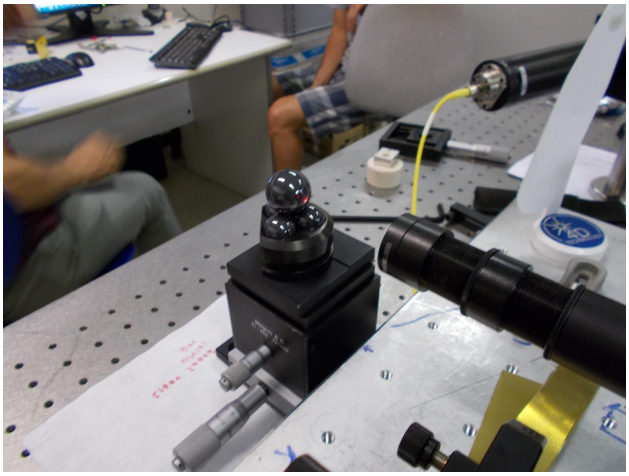

Figure 9. Commercial random ball on its mount during the test measurement of the lens system (the optical tube on the right side).

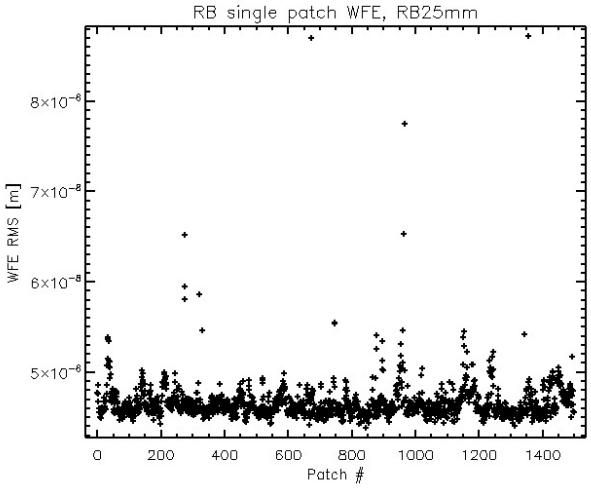

Figure 10. WFE of the measurement patches of the random ball.

5.2 LS measurement

The RB has been mounted with its support on a X,Y stage (lateral and vertical displacement). The setup is shown in Fig. 9. As stated, the RB was sitting on three sphere to allow a smooth rotation around its center. The system focus was adjusted by moving the interferometer and the LS, and the residual power was digitally subtracted.
After alignment, we tested the RB rotation while checking on the interferometer screen that the current fringes density did not exceed the capture range (i.e. we checked that the alignment was effectively preserved while moving). We then collected a sequence of 1500 frames at the interferometer frame rate (25 Hz) while the RB was rotated. The data processing was performed according to the following procedure: as first, the frames have been checked for reconstruction errors due to instantaneous loss of alignment during the sampling; with the valid frames we computed the measurement mask; then we evaluated the dataset average, after removing from each image the alignment modes, namely piston, tip/tilt, focus and coma; at last we evaluated the pixel-wise standard deviation map of the sample.
The resulting average map is shown in Fig.11: under the assumption that the RB contribution is averaged out with the large sampling, the image represents the calibration map of the cavity produced by the LS. In Fig.12 we show the pixel-to-pixel sample standard deviation, whose mean value over the map is 0.4 nm.

A further assessment on the RBT is given by the measurement of the WFE over the local patch viewed by the interferometer. In Fig. 10 we show the sample of the WFE values corresponding to the 1500 frames measurement run. Apart from few points with a local WFE of 70 to 90 nm RMS (likely due to very local imperfections), the typical roughness is lower than 50 nm RMS. When considering the total number of averaged frames (1500) the expected standard deviation is 45 nm/$\sqrt{1500} \approx 1$ nm RMS, which is comparable to the pixel-to-pixel computation. The residual deviation from that value will be addressed in a following step. The activity demonstrated that the RBT is a viable strategy for the calibration of the LS in the OTT, providing a sub-nanometer accuracy of the interferometric cavity.

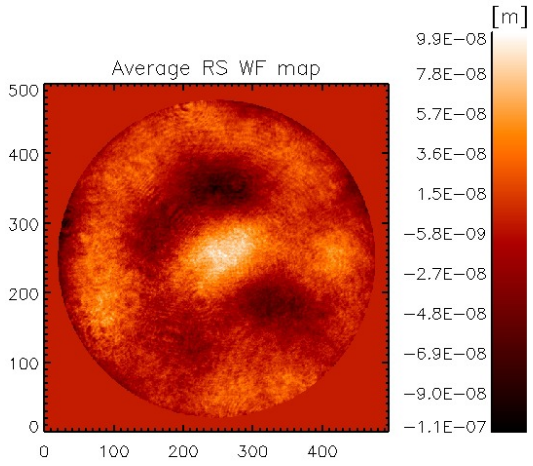

Figure 11. WF of the lens system, obtained after averaging 1500 frames while the RB was rotated

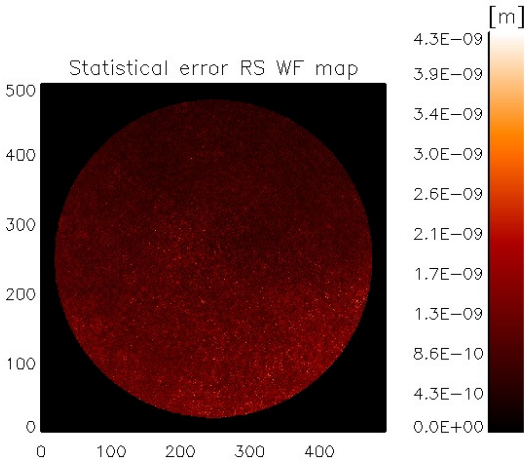

Figure 12. Map of the standard deviation computed pixel-wise on the dataset.

6. DISCUSSION AND CONCLUSION

The optical calibration of the E-ELT M4 mirror on its test bed will be a challenging task never attempted before. Although the optical test concept (including design and procedure) has been kept as simple as possible, the very tight performance requirements needed some innovative approaches. We implemented a risk mitigation strategy, based on the laboratory assessment of some key elements to be deployed and operated in the test tower.

We performed the Random Ball Test to measure with sub-nanometer accuracy the lens system: we arranged a measurement setup and operated it, identifying the key-elements to run it correctly. We tested the interferometer response in presence of spider arms with varying thickness; we investigated how the system returns phasemaps divided into separated islands, as a function of the current fringes density and geometry, spider thickness and modulation threshold set. At last, we checked the procedures for the alignment of the lens system and to operate and test the SPL to measure and recover the initial differential piston error amongst the shells.

The optical test tower will be manufactured, assembled and verified in mid- 2019, to be ready for the optical calibration of M4 two years later.

REFERENCES

[1] Pariani, G., Briguglio, R., Xompero, M., and al., "Optical calibration of the ELT: design, alignment and verification of the interferometric test tower," in [*Proceedings of the Fifth AO4ELT Conference*], (July 2017).

[2] Briguglio, R., Pariani, G., Xompero, M., and al., "Optical calibration of the E-ELT adaptive mirror M4: testing protocol and assessment of the measurement accuracy," in [*Proceedings of the Fifth AO4ELT Conference*], (July 2017).

[3] Xompero, M., Briguglio, R., Pariani, G., and al., "Optical calibration of the ELT: strategy for the optical measurement error estimation," in [*Proceedings of the Fifth AO4ELT Conference*], (July 2017).

[4] Briguglio, R., Pariani, G., Xompero, M., Riccardi, A., Tintori, M., Lazzarini, P., and Spanò, P., "8s, a numerical simulator of the challenging optical calibration of the E-ELT adaptive mirror M4," in [*Adaptive Optics Systems V*], *Proc. of SPIE* **9909**, 99097A (July 2016).

[5] Briguglio, R., Xompero, M., Riccardi, A., and al., "Optical calibration of the M4 prototype toward the final unit," in [*Proceedings of the Fourth AO4ELT Conference*], (Nov. 2015).

[6] Zhou, P. and Burge, J. H., "Limits for interferometer calibration using the random ball test," in [*Optical Manufacturing and Testing VIII*], *Proc. of SPIE* **7426**, 74260U (Aug. 2009).